Analytical Biochemistry 503 (2016) 41–49

Contents lists available at ScienceDirect

Analytical Biochemistry

journal homepage: www.elsevier.com/locate/yabio

Surface plasmon resonance biosensor assay for the analysis of small-molecule inhibitor binding to human and parasitic phosphodiesterases

Marco Siderius [a, *, 1], Anitha Shanmugham [b, 1], Paul England [b], Tiffany van der Meer [a], Jan Paul Bebelman [a], Antoni R. Blaazer [a], Iwan J.P. de Esch [a, b], Rob Leurs [a, b]

[a] Amsterdam Institute of Molecules, Medicines and Systems (AIMMS), Division of Medicinal Chemistry, VU University Amsterdam, De Boelelaan 1083, 1081 HV Amsterdam, The Netherlands
[b] IOTA Pharmaceuticals, St. John's Innovation Centre, Cowley Road, Cambridge CB4 0WS, United Kingdom

ARTICLE INFO

Article history:
Received 4 December 2015
Received in revised form
14 March 2016
Accepted 18 March 2016
Available online 28 March 2016

Keywords:
Phosphodiesterase
Surface plasmon resonance
Small molecules
Trypanosoma brucei
African sleeping disease

ABSTRACT

In the past decade, surface plasmon resonance (SPR) biosensor-based technology has been exploited more and more to characterize the interaction between drug targets and small-molecule modulators. Here, we report the successful application of SPR methodology for the analysis of small-molecule binding to two therapeutically relevant cAMP phosphodiesterases (PDEs), *Trypanosoma brucei* PDEB1 which is implicated in African sleeping sickness and human PDE4D which is implicated in a plethora of disease conditions including inflammatory pulmonary disorders such as asthma, chronic obstructive pulmonary disease and central nervous system (CNS) disorders. A protocol combining the use of directed capture using His-tagged PDE_CDs with covalent attachment to the SPR surface was developed. This methodology allows the determination of the binding kinetics of small-molecule PDE inhibitors and also allows testing their specificity for the two PDEs. The SPR-based assay could serve as a technology platform for the development of highly specific and high-affinity PDE inhibitors, accelerating drug discovery processes.

© 2016 Elsevier Inc. All rights reserved.

Introduction

Among the various enzymes involved in regulation of cellular signal transduction, 3′,5′-cyclic nucleotide phosphodiesterases (PDEs) are of interest as they play an important role in regulation of the cellular levels of the ubiquitous secondary messengers, cyclic guanosine monophosphate (cGMP) and cyclic adenosine monophosphate (cAMP). These secondary messengers control a range of cellular processes, including the production of inflammatory mediators, apoptosis, ion-channel function and cellular differentiation [1,2]. Eleven PDE super-families, encompassing several gene products and splice variants, have now been identified in human. These families are mainly distinguished based on their substrate specificity, inhibitor potency, cellular distribution and domain architecture. PDE inhibitors such as sildenafil (PDE5-selective) for the treatment of erectile dysfunction [3] and roflumilast (PDE4-selective) for treatment of chronic obstructive pulmonary disease (COPD) [4] are currently on the market. Modulation of human PDE4 (hPDE4) subtypes is therapeutically interesting for the treatment of a plethora of disease conditions including inflammatory pulmonary disorders such as asthma, COPD and central nervous system (CNS) disorders (e.g. Alzheimer's disease) [5].

Recently, parasitic PDEs have emerged as targets for the treatment of important neglected parasitic diseases [6] such as human African trypanosomiasis (HAT), Chagas disease and Leishmaniasis. HAT, also called African sleeping sickness, is a neglected tropical disease (NTD) that is endemic in several developing countries [7] and is caused by the parasite *Trypanosoma brucei*. Two highly homologous PDEs, *Tbr*PDEB1 and *Tbr*PDEB2 are essential for the virulence of *T. brucei* [6,8]. The ablation of both parasitic PDEs using RNAi results in accumulation of intracellular cAMP and eventually to cell cycle defects and cell death in bloodstream form trypanosomes [6,8], making these PDEs attractive drug targets for the treatment of HAT.

* Corresponding author.
E-mail address: m.siderius@vu.nl (M. Siderius).
[1] These authors contributed equally to this work.

http://dx.doi.org/10.1016/j.ab.2016.03.013
0003-2697/© 2016 Elsevier Inc. All rights reserved.

To facilitate the discovery of novel drug-like molecules targeting specific PDEs, understanding the dynamics of interaction between small-molecule modulators and the protein target has gained significant recognition [9]. Consequently, surface plasmon resonance (SPR) biosensor-based technology is increasingly utilized to characterize bio-molecular interactions, allowing the simultaneous evaluation of both kinetic [10] and thermodynamic parameters [11]. Generally, in an SPR biosensor-based assay, one interaction partner is immobilized on a sensor chip and exposed to the other interaction partner that is brought into contact with the chip surface in flow. The SPR readout of a binding event is determined by changes in the mass or refractive index of the surface layer. Immobilization of a low molecular weight (MW) interaction partner and flowing of the higher MW interaction partner such as proteins will increase the possibility of a measurable response upon interaction. This approach was earlier applied in PDE research, where SPR imaging for PDE5 was performed on arrays comprising of immobilized compounds [12]. However, this strategy suffers some serious drawbacks such as large mass transfer effects due to slow diffusion of the PDE enzyme in the layers of solution flowing over the sensor chip and dextran matrix on the surface, and the significant entropic cost upon immobilizing the faster diffusing small molecules. Moreover, a major issue when using this approach is the need to choose an attachment site that does not disturb the interaction for all the small molecules subject to study. Hence, it is preferable to immobilize the protein target in these assays. With the increased sensitivity of modern SPR instrumentation (Biacore T200, GE Healthcare), this technology has been successfully extended to study small-molecule (<300 Da) binding to an immobilized protein surface [13]. While kinase-targeted drug discovery has been benefiting from the latter approach [14–16], no such methods have so far been described for targeting PDEs. In this study, we describe the development of an SPR biosensor-based assay for *Tbr*PDEB1 and hPDE4D, two therapeutically relevant targets. We have expressed, purified and immobilized the catalytic domain of both PDEs to investigate the dynamic interactions of small-molecule PDE inhibitors that were generated during our effort to identify next-generation therapeutics for the treatment of NTDs such as HAT [8,17,18].

Results and discussion

Expression, purification and functional characterization of TbrPDEB1 and hPDE4D catalytic domains

Like all PDEs, hPDE4D and *Tbr*PDEB1 contain a conserved C-terminal catalytic domain, but differ in their family-specific N-terminal regulatory domains [1]. While the N-terminal regulatory region of hPDE4D consists of tandem UCR (Upstream Conserved Region) domains, its *Tbr*PDEB1 counterpart consists of tandem GAF (derived from the first three identified proteins comprising this domain: cGMP-binding phosphodiesterases, cyanobacterial Adenylyl cyclases, and a Formate-hydrogen lyase transcription activator from *Escherichia coli*) domains. Although the N-terminal regulatory domains are important for regulation of PDE functionality [2,19–21], the catalytic domain (CD) alone is known to be responsible for the enzymatic activity of these enzymes. Consequently, the CD contains all structural elements to mediate hydrolysis of the cyclic nucleotide 3′,5′-phosphodiester bond. Moreover, the CD has so far been the targeting site for most of the reported PDE inhibitors [22]. Recently, also the structural properties of the CD of hPDE4 and *Tbr*PDEB1 were explored as they could be purified and subsequently crystallized, facilitating structure – function relationship studies of small-molecule interaction with the catalytic site [23,24]. To establish an SPR biosensor-based approach with immobilized PDEs, we focused on the CD of hPDE4D and *Tbr*PDEB1. Accordingly, we expressed recombinant 6xHis-tagged CDs in *E. coli* that subsequently could be purified in a single step Ni-NTA column procedure (Fig. 1A). In this way, we were able to obtain 5 mg of each purified His-tagged PDE from 1 L of culture volume. Purified samples (15 μg each) were analysed on SDS–PAGE. The isolated CDs displayed the expected mobility for the CDs of hPDE4 and *Tbr*PDEB1, running at 42 kDa and 37.5 kDa, respectively (Fig. 1B). The purity of both samples was estimated to be 80–85%. To investigate the functionality of the CDs of both isolated PDEs, we used a bioluminescence assay (Lonza, Rockland USA) to evaluate cAMP phosphodiesterase activity. The enzymatic activity of the isolated CDs at various time points of incubation at 25 °C was investigated (0, 1, 2, 5, 25 and 50 h, Fig. 1C). Activity of hPDE4D_CD remained unaltered over a 50 h time span. In contrast, *Tbr*PDEB1_CD retained reasonable levels of activity until the 5 h time point. The reduced stability of the *Tbr*PDEB1_CD may have implications for the life span of the PDE biosensor surface.

A strategy for capturing PDE_CD on a Biacore sensor surface is to make use of the His-tag attached to the PDE proteins. Immobilizing the PDE_CD using the His-tag requires a nickel-treated nitrilotriacetic (Ni^{2+}-NTA) surface. Capturing a ligand on a Ni^{2+}-NTA surface may result in nonspecific binding as a consequence of residual Ni^{2+} present on the surface. A wash step with EDTA in the running buffer to remove excess nickel from the surface would provide a means to prevent nonspecific binding on the SPR surface. To explore the possibility of incorporating an EDTA wash step in the capturing protocol, the sensitivity of PDE_CD activities to EDTA was investigated. As shown in Fig. 1D, hPDE4D_CD was resistant to EDTA exposure. In contrast, the *Tbr*PDEB1_CD is very sensitive to EDTA, loosing about 90% of its activity (Fig. 1D). However, *Tbr*PDEB1_CD activity could be restored adding 0.5 mM Zn^{2+} and 0.5 mM Mg^{2+} salts in combination, restoring full activity of the enzyme.

To investigate whether the PDE activity associated with the isolated hPDE4D and *Tbr*PDEB1 CDs could still be modulated, phosphodiesterase activity in the presence of two inhibitors, rolipram and VUF13524, was assayed in the bioluminescence assay. As is clear from Fig. 1E, VUF13524 inhibited both PDE_CDs (IC_{50} *Tbr*PDEB1_CD; 0.25 μM, PDE4D_CD; 0.055 μM), whereas rolipram affected hPDE4 functionality (IC_{50} 2 μM) but not *Tbr*PDEB1 as described earlier [25].

In conclusion, we were able to isolate the CD of both hPDE4D and *Tbr*PDEB1 in an active form to set up a protocol to functionally capture PDEs on a Biacore sensor surface.

Preparation of a PDE_CD SPR biosensor surface

The standard hPDE4 inhibitor rolipram, along with the recently discovered *Tbr*PDEB1 inhibitor VUF13524 and two analogues [17] were used in our SPR analyses. Their inhibitory potencies (IC_{50} values) for the CD-only preparations of hPDE4D and *Tbr*PDEB1 are provided in Table 1. The PDE inhibitor series used here, exhibit a broad range of potencies varying from about 300-fold range for hPDE4D to over 10,000-fold for *Tbr*PDEB1, an interesting feature that enables them as tools to explore the dynamic range of a SPR-based PDE assay. For initial optimization of the PDE_CD sensor surface, VUF13524 was used as analyte (Fig. 2A).

Using the Biacore T200 system, it is possible to simultaneously evaluate the interaction of small molecules with four different sensor surfaces on a single chip. We designed our chip comprising a blank and 3 protein immobilized sensor surfaces: hPDE4D_CD, *Tbr*PDEB1_CD and a reference protein. As reference, we used recombinant His-tagged TorD, a nucleotide-binding chaperone from *E. coli* [26]. In all our analyses, no interaction of TorD with PDE ligands was observed (data not shown). Functional capturing of

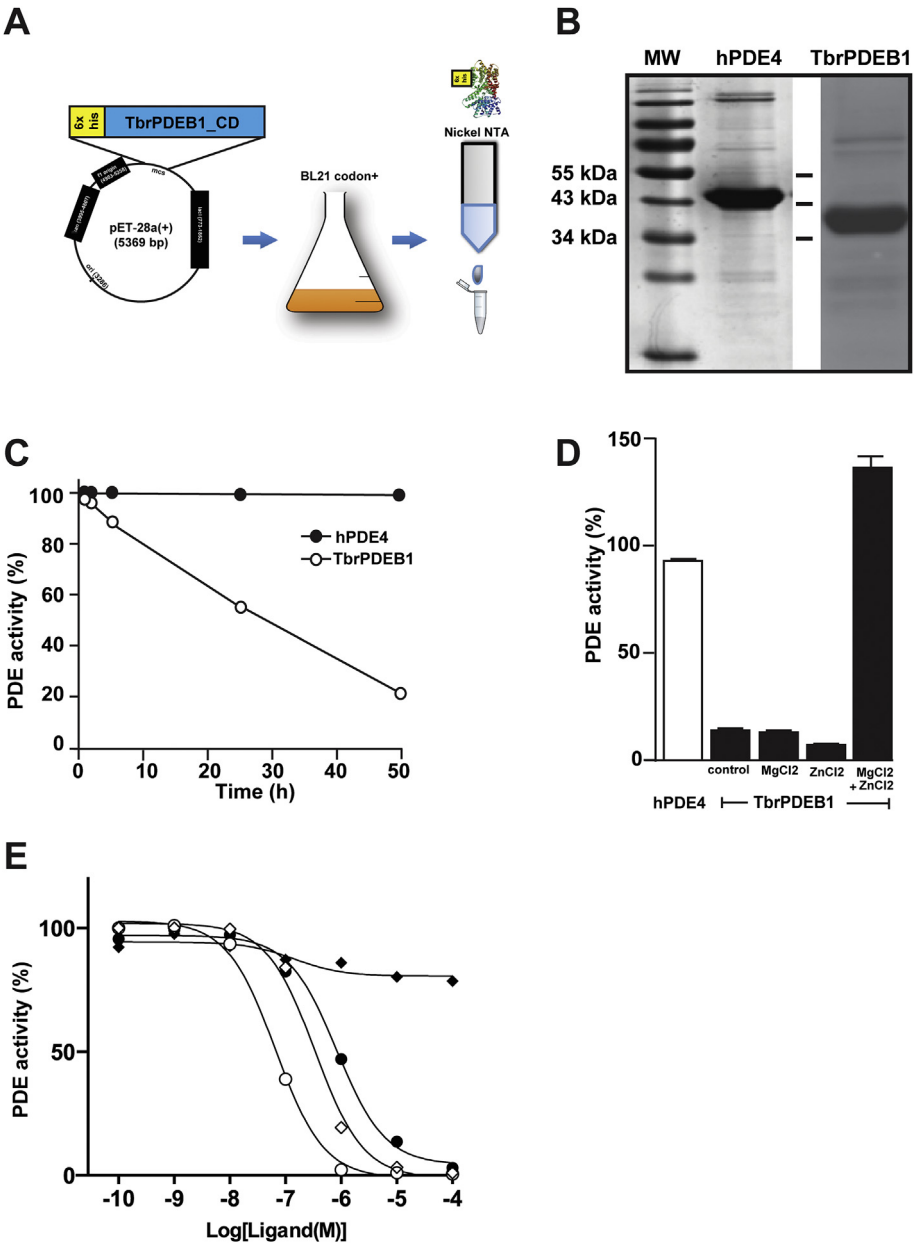

Fig.1. A. Heterologous expression His-tagged catalytic domains of hPDE4D_CD and *Tbr*PDEB1_CD. His-tagged catalytic domains (PDE_CD) were cloned into the pET28a (+) vector and transformed to the BL21 bacterial strain. Transformed bacteria were cultured in 1 L cultures after which the His-tagged PDE_CDs were purified in a one-step purification procedure using a Ni-NTA column. B. Qualitative analysis of purified His-tagged PDEs. Single-step, Ni-NTA column purified samples of His-tagged hPDE4D_CD (42 kDa) and *Tbr*PDEB1_CD (37.5 kDa), each 15 μg were analysed separately by 10% SDS–PAGE gel. Lane MW: molecular weight marker. C. Determination of stability of PDE activity over time using bioluminescence assay. Activities over time of hPDE4_CD and *Tbr*PDEB1_CD incubated at 25 °C as measured using the bioluminescent assay (Lonza) is displayed. Under the provided experimental conditions, hPDE4_CD seems to have a very stable activity whereas *Tbr*PDEB1_CD gradually looses activity over a period of 50 h. D. EDTA interferes with enzymatic activity of PDEs. PDE activity as measured using the bioluminescent assay following incubation with 20 mM EDTA for 30 min at 25 °C. While hPDE4D_CD (White bar) seems not affected, *Tbr*PDEB1_CD (Black Bar, control) lost about 90% of its activity. Recovery of *Tbr*PDEB1_CD activity was achieved by adding co-factors Mg^{2+} and Zn^{2+} in form of divalent salts. Addition of 0.5 mM $MgCl_2$ and 0.5 mM $ZnCl_2$ separately fails to stimulate activity of EDTA-inactivated *Tbr*PBEB1_CD, however when used in combination *Tbr*PDEB1_CD reactivation to untreated level is apparent. E. Inhibition of hPDE4D_CD and *Tbr*PDEB1_CD activity by rolipram and VUF13524. The PDE activity of hPDE4D_CD (circles) and *Tbr*PDEB1_CD (diamonds) was assayed in the bioluminescent assay (Lonza). Activity was measured during 20 min after preincubating the PDE_CD with rolipram (closed symbols) and VUF13524 (open symbols), respectively, for 15 min at 25 °C. PDE activity is depicted as percentage of the uninhibited activity.

PDE_CD onto a SPR biosensor surface was optimized in three steps as indicated in Fig. 2A. Initially, direct amino coupling on a CM5 surface was tested (2A, I). Capturing the PDE_CD on CM5 surface using the standard Biacore protocol (employing the cross-linking reagents EDC and NHS), we managed to immobilize about 2500 Resonance Units (RUs) of both proteins. The hPDE4D_CD and *Tbr*PDEB1_CD surface was stable during the first 50 h as could be concluded from the absence of a baseline shift during this time period (Fig. 2B).

Moreover, clear signals were obtained upon interaction with of our analyte (VUF13524). However, the observed B_{max} differed a lot from the calculated B_{max}, indicating that capturing the PDE_CD had impaired the possibility to interact with VUF13524 (34% and 2% residual B_{max} for hPDE4D and *Tbr*PDEB1, respectively). Exposure of PDE_CDs to the non-native coupling conditions during immobilization could have likely interfered with their physical properties. Moreover, the amino acid residue(s) involved in the random-coupling immobilization strategy are not exactly predictable and

Table 1
PDE_CD-interacting compounds inhibiting hPDE4_CD and TbrPDEB1_CD catalytic activity as measured in the bioluminescent assay (IC_{50}). Affinities of the same compounds as measured with SPR assay (K_D). The error of the K_D reported in the table, is the error in the fit of the binding isotherm.

Compound	hPDE4D_CD IC_{50} (M)	K_D	*Tbr*PDEB1_CD IC_{50} (M)	K_D
Rolipram	2.03E-06	2.08 ± 0.24E-06	>>2E-03	>>2E-03
VUF13524	5.52E-08	1.30 ± 0.13E-07	2.54E-07	1.24 ± 0.33E-07
VUF13525	6.80E-09	5.70 ± 0.16E-08	5.46E-08	2.25 ± 0.36E-08

in some case may reside in a site near the analyte binding pocket thereby altering or blocking binding.

To improve functionality of the PDE_CD biosensor surface, we utilized the His-tag to directly capture PDE_CD on a Ni^{2+}-NTA surface (Fig. 2A, II). This method yielded a surface that behaved properly in terms of the B_{max} upon interaction with VUF13524, which was in close correlation with the theoretical value (Fig. 2C, 102% and 72% B_{max} for hPDE4D and *Tbr*PDEB1, respectively). However, using the Ni^{2+}-affinity capturing strategy, the surface appeared unstable as can be concluded from the relatively large baseline shift that was apparent for the two PDE surfaces (Fig. 2C). A solution to decaying surfaces was earlier suggested by Joss et al. [27] who developed computational methods to correct for the baseline drift. Unfortunately, the decay effect observed for the PDE surfaces is too large in comparison to the small signals that are obtained in studies with small molecules prohibiting kinetic analyses.

Therefore, we next performed a covalent stabilization step of the captured His-tagged PDEs adapting a recently developed protocol for generating a stable and active sensor surface for recombinantly expressed, His-tagged cyclophilin A to study small molecule interactions [28]. In this method, His-tagged PDEs are captured directly to the Ni^{2+}-activated NTA sensor chip surface without exposing the PDEs to adverse buffers to pre-concentrate and the surface is thereafter activated with an EDC/NHS mixture. In this method, the His-tag serves to non-randomly orient the target PDE_CDs onto the surface for subsequent covalent cross-linking via the activated carboxyl groups of the chip surface. This method is much milder than the standard "low-salt, low-pH" pre-concentration step for amine coupling. Due to the oriented immobilization the functionality of the ligand-binding pocket will most likely not be affected by any surface-mediated steric hindrance effect [29]. We adapted this protocol in an attempt to control the cross-linking step by specifically targeting the EDC/NHS activation towards the carboxyl groups on the sensor surface and avoid any carboxyl groups on PDE_CD. This could be achieved by shifting the EDC/NHS-surface activation step prior to injection of PDE_CDs. Following surface activation the EDC/NHS mixture is washed off by buffer and will thus not affect the PDE_CD that is injected later. This procedure should restrict any possible intra- or inter-molecular PDE_CD cross-links that may lead to inactivation of e.g. *Tbr*PDEB1_CD (Fig. 2B). When PDE_CD is presented to the surface, it gets captured to the Ni^{2+}-activated NTA moiety bringing them close to the already activated carboxyl groups on the sensor surface. As a result, the Ni^{2+}-NTA captured His-tagged protein is simultaneously covalently coupled to the surface via other amino acids (Fig. 2A, III). Using this protocol, we were able to generate a stable surface exhibiting binding responses that indicate functionality of both the immobilized hPDE4D_CD (86% of the theoretical B_{max}) and *Tbr*PDEB1_CD (32% of the theoretical B_{max}) (Fig. 2D). Removal of excess Ni^{2+} from the sensor surface by means of an EDTA wash and subsequent regeneration step with Zn^{2+} and Mg^{2+} salts (0.5 μM each) of the PDE_CD surface did not alter the VUF13524 binding capacity of both hPDE4D_CD and *Tbr*PDEB1_CD (data not shown).

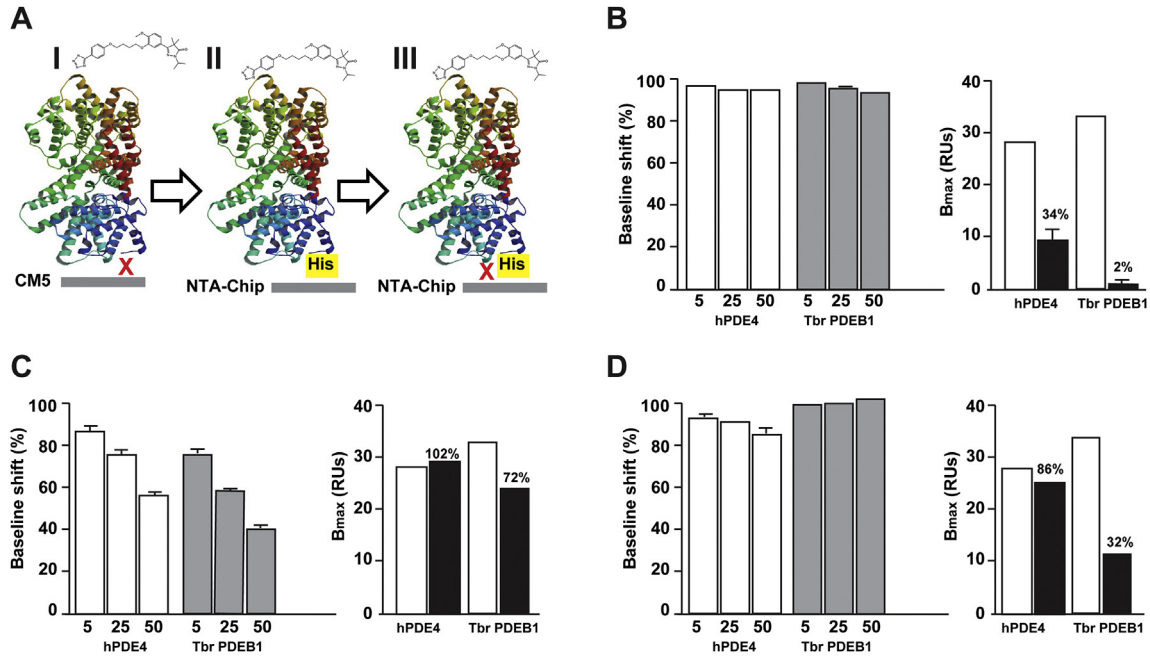

Fig.2. PDE sensor surface generated by various coupling methods. A. PDE catalytic domains were immobilized on (I) CM5 chips by amide coupling, (II + III) NTA chips by His- Ni-NTA affinity capture alone (II) or followed by amide coupling (III), respectively. Analysis of the surface functionality is performed using 1 μM VUF13524 as analyte in all assays. B–D, Analysis of surface stability of different immobilization protocols (B; protocol I, C; protocol II, D; protocol III) was performed over 5, 25 and 50 h after surface generation (left graphs). Stability was determined as the percentage of baseline shift compared with the surface at 0 h (hPDE4_CD, white bars, *Tbr*PDEB1_CD grey bars). The percentage baseline shift is a product of averaging three independent normalized observations. The binding of VUF13524 to the immobilized surfaces (right graphs) is represented as the average of maximum binding responses (B_{max}) following normalization. White bars represent the B_{max}, calculated based on MW of the ligand and analytes, and the amount of RU of captured ligand. Black bars depict the observed B_{max} as percentage of the calculated B_{max}.

Functionality of immobilized PDE_CD over time

Producing a sensor chip with a long operational life is highly desirable to study interactions with many small molecules at various concentrations. To estimate operational life of the PDE_CD surfaces, 1 μM VUF13524 was injected at variable time points (1–25 h) and the binding signal output was studied (Fig. 3). For hPDE4D_CD, the binding capacity for 1 μM VUF13524 is relatively stable over the 25 h period in presence of 5% glycerol in the running buffer. We measured a 20% loss of binding capacity during the first 20 h but afterwards the binding capacity remains stable (Fig. 3A). On the other hand, the binding capacity of *Tbr*PDEB1_CD deteriorates rapidly over time even in the presence of 5% glycerol (Fig. 3B). In the first 2 h, roughly 50% of the binding capacity is lost and in more than 90% of the binding capacity is lost in 5 h (Fig. 3B). In contrast to hPDE4_CD, the use of *Tbr*PDEB1_CD surfaces is therefore only possible for a limited amount of time. This likely is due to the general instability of this catalytic domain construct as also was exemplified in Fig. 1C.

Interaction hPDE4D_CD, TbrPDEB1_CD sensor surfaces with cAMP

After optimizing the surfaces with the PDE inhibitor VUF13524, we analysed the PDE_CD biosensor surface for binding the PDE native substrate cAMP. Both *Tbr*PDEB1_CD and hPDE4D_CD show concentration-dependent increases in binding responses to cAMP (Fig. 4A and B). Interestingly, the sensorgrams are different for the two PDEs. While the *Tbr*PDEB1_CD surface shows rapidly saturating binding curves (Fig. 4A), the hPDE4D_CD surface shows a rapid phase followed by a slow binding phase (Fig. 4B) for the cAMP concentrations studied. Moreover, the dissociation phase observed on *Tbr*PDEB1_CD surface seems monophasic while on hPDE4D_CD surface a bi-phasic, a fast and a slow dissociation phase were observed. Enzyme-substrate interactions often comprise of a complex series of steps: binding of the substrate (cAMP), possible conformational changes within the enzyme, substrate hydrolysis, product (AMP) formation and release. We do not know the rate-determining step(s) that determines the overall kinetics for cAMP hydrolysis by PDEs and therefore it is impossible to solve the interaction mechanism by use of appropriate binding models. However, by plotting the SPR responses at equilibrium (R_{eq}) for each sensorgram against the respective concentration of cAMP and non-linear fitting, affinity constants (K_D values) were extracted (not shown). The extracted K_D values of hPDE4D_CD and *Tbr*PDEB1_CD, 7.4 μM and 7.7 μM are very similar, and also in the range of the observed K_m values for these PDEs [30–32].

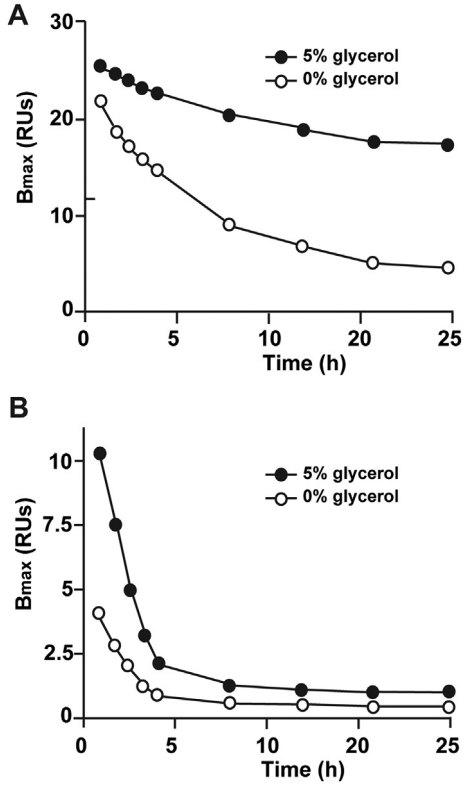

Fig.3. Binding capacity of PDE-based sensors over time. Stability of PDE surfaces (hPDE4_CD (A), *Tbr*PDEB1_CD (B), prepared as in Fig. 2A; III) was analysed using 1 μM VUF13524 injected at variable time points (1–25 h) as analyte. A comparison was made in presence (closed symbols) and absence (open symbols) of 5% glycerol.

Affinity analysis of PDE inhibitors using the PDE_CD based SPR assay

Subsequently, we used the PDE-based SPR sensor to directly and quantitatively study the affinity of rolipram, a known inhibitor of hPDE4 function. In these experiments, the analyte typically was injected at variable concentrations. The injection time was kept short (60 s) and the dissociation phase was long enough to allow complete dissociation of the analyte from the sensor surface. Sensorgrams of the binding of rolipram were recorded for a series of concentrations (Fig. 5 A, *Tbr*PDEB1_CD (blue), B hPDE4D_CD (pink)). The curves shown in Fig. 5C represent steady-state affinity analysis of rolipram binding to hPDE4D fitted to a 1:1-interaction model (pink), the data points obtained for the TbrPDEB1 surface were not fitted (blue). The observed K_d value that can be extracted from the SPR analysis is within the same quantitative range (around 10^{-6}) as the IC_{50} values obtained in the enzymatic assays (2×10^{-6}). Next, we used the PDE-based SPR sensor to directly and quantitatively study the affinity of two inhibitors (VUF13524, VUF13525) characterized in a previous study [17]. The sensograms of binding of VUF13524 (blue sensorgrams) and VUF135252 (red sensorgrams) are depicted in Fig. 6 A (*Tbr*PDEB1) and C (hPDE4D). Steady state affinity analysis of the interactions 2 s before the end of the injections, were fitted to a 1:1 interaction model for *Tbr*PDEB1 (B) and hPDE4D (C). Notably, although fitting of the steady affinities for these compounds is very comparable, the kinetics of interaction of VUF13525 with hPDE4D seems slower both in association as in dissociation compared to *Tbr*PDEB1 interaction, underscoring the added value of biophysical analysis of small molecule-drug target interactions. Differences in association and dissociation kinetics of different PDE inhibitors may reflect different interactions with the protein target that may be further exploited to improve the molecules in a drug development program. Especially in combination with structural information about the interaction of the molecules with the target, biophysical data may steer the development of new molecules with desired kinetic characteristics.

Conclusions

In conclusion, our PDE based-SPR assay enabled direct measurement and extraction of the equilibrium dissociation constants of inhibitor binding, which are otherwise difficult to measure using other available *in vitro* techniques. The catalytic domains from two different phosphodiesterases, *Tbr*PDEB1 and hPDE4D have been utilized in our SPR assay. For both the enzymes the immobilization steps were optimized to yield moderate (for *Tbr*PDEB1_CD) to high (for hPDE4D_CD) surface activity, a critical step that is often a limiting factor in the development of biosensor methods. Improvement of use of the SPR-based technology may be achieved

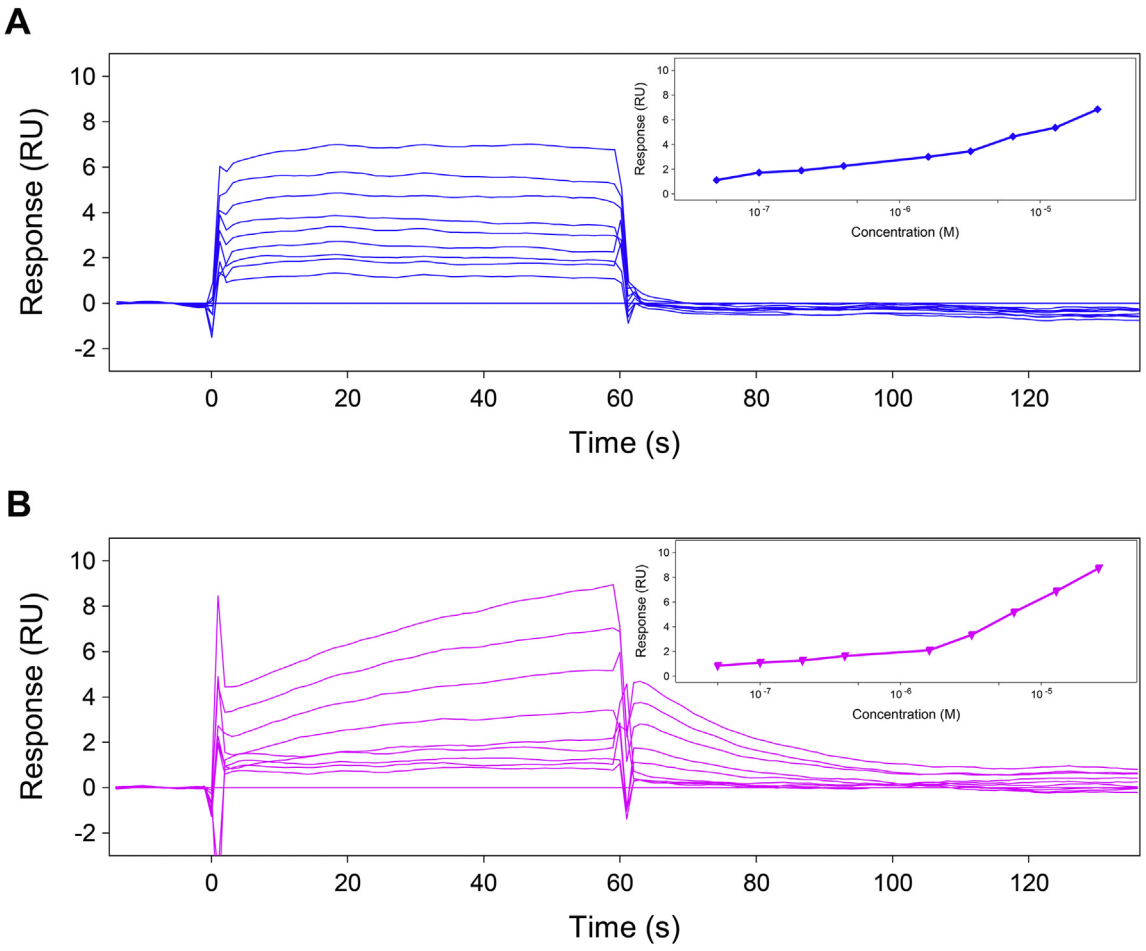

Fig.4. SPR analysis of cAMP binding to *Tbr*PDEB1_CD and hPDE4D_CD. PDE surfaces as prepared using the capturing method described in Fig. 2A, III, were used to examine binding of cAMP (concentrations) to the catalytic domains of *Tbr*PDEB1_CD (A) and hPDE4D_CD (B). Inserts represent the dose–response curves for both assays measured 2 s before the end of the injections.

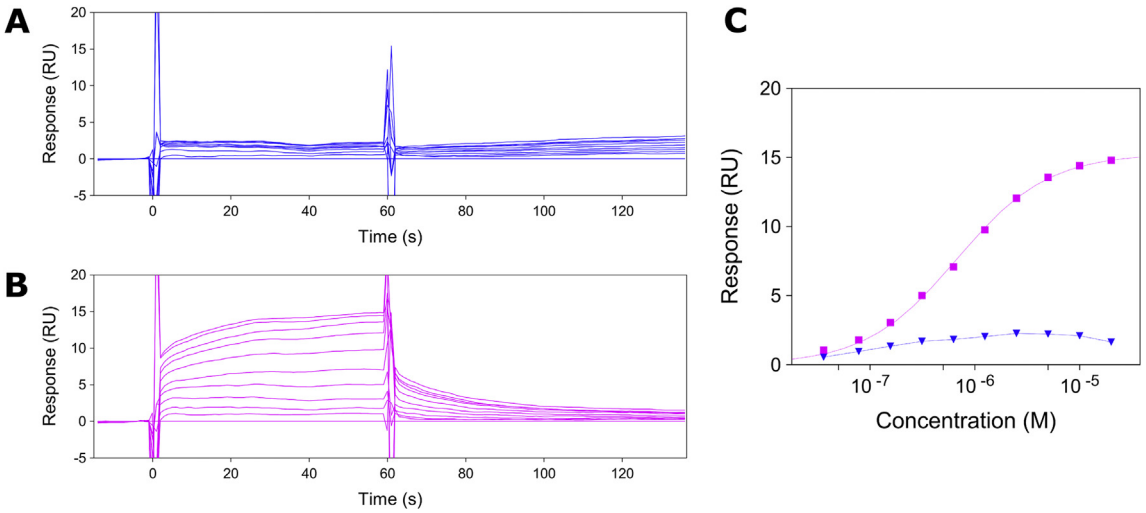

Fig.5. Binding of rolipram to hPDE4D_CD sensor surface. The sensorgrams of SPR analysis of binding of rolipram to *Tbr*PDEB1 (A) and hPDE4D (B) are plotted. C. Steady-state affinity analysis of rolipram binding to hPDE4D fitted to a 1:1-interaction model, the data points obtained for the TbrPDEB1 surface were not fitted.

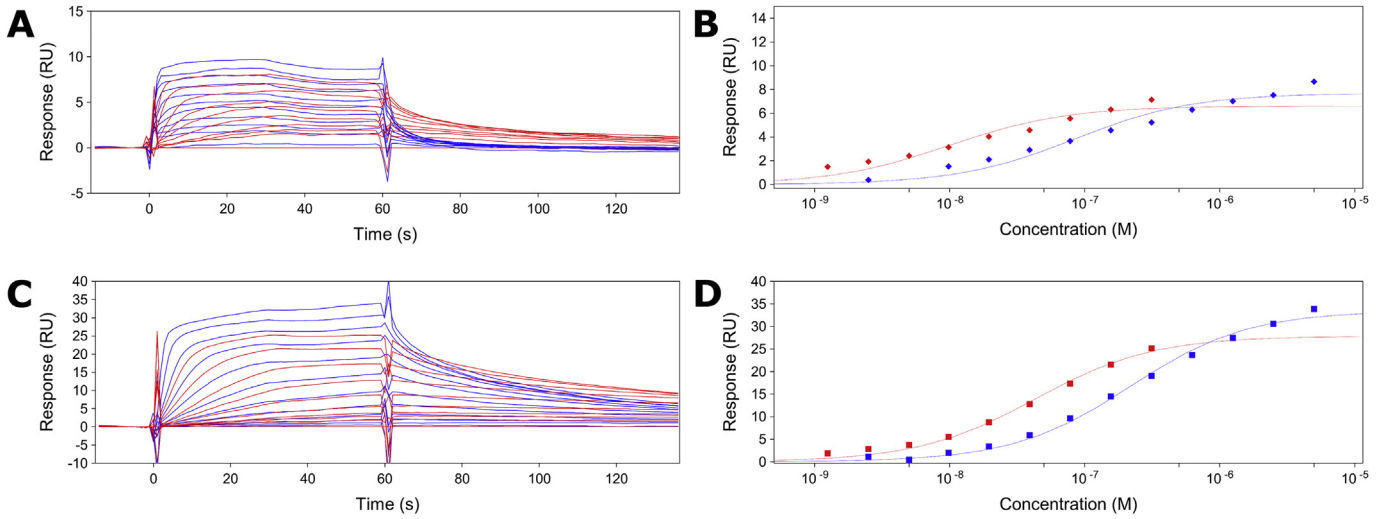

Fig.6. Binding of VUF13524, VUF135252 to the *Tbr*PDEB1_CD and hPDE4D_CD sensor surface. Binding of VUF13524 (blue) and VUF13525 (red) to *Tbr*PDEB1_CD (A) or hPDE4D_CD (C), with a steady-state affinity analysis of responses at 2 s before the end of injections, fitted to a 1:1-interaction model (Scrubber) for TbrPDEB1 (B) and hPDE4D (D). The error reported is the error in the fit of the binding isotherm. (For interpretation of the references to colour in this figure legend, the reader is referred to the web version of this article.)

by increasing the surface stability, especially for the *Tbr*PDEB1_CD. This could be done by selection of a different CD domain construct or by expression of the full-length protein that may be more stable. Alternative methods of capturing the protein to the surface, *e.g.* biotinylation and capture on streptavidin-coated surface, may also be explored.

The equilibrium analysis of various small-molecule inhibitors seemed to yield reasonable qualitative correlation of affinity rates with the known IC_{50} values. The measurement of the affinity of small molecules for the PDE_CD by this SPR-mediated assay will increase our toolbox for drug discovery. Further exploiting the possibilities of this biophysical tool may serve to extract valuable parameters (kinetics) of small molecule drug target interactions generating added value as a technology platform for drug discovery.

Materials and methods

Subcloning, expression and purification of recombinant proteins

The catalytic domain of hPDE4D (380–756, codon optimized) was synthesized and subcloned into expression vector pET15b (Genscript). The plasmid pET-PDEB1, previously reported by Jansen et al. [24] was used for expression of His-tagged *Tbr*PDEB1 (586–918; catalytic domain). The plasmid pET16b-TorD, previously reported by Shanmugham et al. [26] was used for expression of His-tagged TorD. The vectors were transferred into *E. coli* strain *BL21* (codon plus) and grown in LB medium at 37 °C to absorption of A_{600} = 0.7 and then 0.2 mM isopropyl β-D-thiogalactopyranoside was added to induce the overexpression at 15 °C for 24 h. Cells are pelleted and resuspended in extraction buffer (20 mM KPO_4, pH = 8, 300 mM NaCl, 1 mM β-mercapthoethanol, 1 mM $MgCl_2$, 0.1 mM $ZnSO_4$ and 10% glycerol). Cells are then disrupted (2 rounds 1500 Bar) in an EmulsiFlex-C3 (Avestin, inc, Germany). Cell debris is pelleted in 2 mL tubes for 10 min at 14,000 rpm. The cell free lysate is centrifuged for 15 min at 14.000 rpm. The cell free lysate is applied to a Ni-NTA column (1 mL Ni-NTA agarose slurry, Invitrogen). Column material is pretreated with 10 column volumes elution buffer (extraction buffer plus 250 mM imidazole) followed by 10 column volumes of binding buffer (extraction buffer plus 20 mM imidazole). Column with bound His-tagged PDE_CD is washed with binding buffer (10 column volumes). Bound protein is eluted with elution buffer in 0.5 mL fractions. To remove imidazole, samples are desalted over a PD10 desalting column (GE Healthcare) and eluted with 50 mM Hepes, pH = 7.8, 300 mM NaCl, 1 mM β-mercapthoethanol, 1 mM $MgCl_2$, 0.1 mM $ZnSO_4$ and 10% glycerol. The purity of the isolated hPDE4_CD and TbrPDEB1_CD was estimated after SDS–PAGE by analysis of the Coomassie-stained gels with Image J 1.50e. Samples are aliquoted, snapfrozen in liquid N_2 and stored at −80 °C.

Bioluminescence assay for measuring PDE activity

The determination of PDE_CD activity was performed with PDELight HTS cAMP phosphodiesterase kit [33,34] developed by Lonza Rockland, Inc. This assay allows a continuous readout of PDE activity based on the following reaction: PDEs hydrolyse cAMP to AMP; AMP is then converted directly to ATP by “AMP-DR”, Lonza's proprietary AMP detection reagent; luciferase is then utilized to catalyse the formation of light from luceferin and the newly formed ATP. The luciferase catalysis step also regenerates AMP, and therefore, the light output is linear with the rate of AMP production by the PDE. From the rate of increase in light intensity over a period of time, the reaction rate is calculated. The reaction output light was monitored at 25 °C for 20 min using $Victor_2$, yielding a specific activity of about 2500 U/min in the given conditions as previously described by us [17]. The PDE reaction buffer is 50 mM Hepes, 100 mM NaCl, 1 mM $MgCl_2$, 0.1 mM $ZnCl_2$, 5% (v/v) glycerol, pH = 7.8. The reaction is performed in 50 μL with cAMP concentrations, 0.5 μM for *Tbr*PDEB1_CD and 1 μM for hPDE4D_CD.

This assay was also used in the determination of IC_{50} values for inhibitors against catalytic domain of PDEs studied. The inhibitors were pre-incubated with PDE_CD comprising 1% (v/v) DMSO in assay buffer and in a 96-well format. Dose–response curves were generated by plotting the percent of inhibition of PDE against the inhibitor concentrations. Nonlinear regression analysis was used to calculate IC_{50} values from each dose–response curve by using GraphPad Prism (version 5.01).

SPR measurements

All experiments were carried out using BIAcore T200 (GE healthcare), at 25 °C and a flow rate of 60 μL/min. The sensor chips CM5 series S and NTA series S and Biacore consumables were

obtained from GE Healthcare. All solutions were freshly prepared, degassed, and filtered through membranes with 0.22 μm pores. The running buffer used was PBS buffer with (v/v) 5% glycerol, 1% DMSO and 0.005% Tween-20 for all the experiments.

Sensor surface preparation for CM5 chip

PDEs were immobilized using the standard amine coupling protocol (Amine Coupling Kit, BR-1000-50, GE Healthcare). The PDEs, hPDE4D_CD (200 μg/mL, diluted in 10 mM acetate, pH 5.6) and *Tbr*PDEB1_CD (200 μg/mL diluted in 10 mM acetate, pH 5.0) were injected to a readout of 2500 response units (RU) on surfaces that had been activated for 7 min with a 1:1 mix of 0.2 M *N*-ethyl-*N*'-(3-dimethylaminopropyl)-carbodiimide HCl (EDC) and 0.05 M *N*-hydroxysuccinimide (NHS). Remaining reactive groups on the matrix were blocked by treatment with 1 M ethanolamine HCl at pH 8.5. An empty control surface was obtained by submitting the reference flow channel to the same protocol as used for target immobilization except that no protein was injected.

Sensor surface preparation for NTA chip

The sensor chip NTA was primed, conditioned with a 1 min injection pulse of 350 mM EDTA, and loaded with 50 μL of 0.5 mM $NiCl_2$ in running buffer was injected to activate the surface. This is followed by injection of His-tagged PDEs (20 nM) in running buffer, except for the reference surface, to which no protein was bound. For qualitative binding studies, PDEs were immobilized to readout of 2500 response units (RU) in order to maximize the sensitivity of the experiment. To remove excess Ni^{2+}, the surface was washed with 20 mM EDTA in running buffer. Regeneration of the PDE surface after the EDTA treatment was performed washing with running buffer supplemented with 0.5 μM of $ZnCl_2$ and $MgCl_2$. In the final protocol (Fig. 2A III), surface activation with Ni^{2+} preceded that with EDC/NHS, after which the PDEs were captured-coupled (~2500 RU), followed by a washing step, the EDTA treatment and recovery of the PDE surface. However, use of the *Tbr*PDEB1_CD surface generated in this manner is limited in time due to deterioration of the captured protein. This surface can be used for approximately 6 h depending on the actual binding capacity R_{max} of the surface. Surfaces with hPDE4D_CD could be used for longer periods of time and have been used reliable for more than 24 h. Regeneration at the end of the dissociation period was not performed for two reasons: (1) all reported analytes were fully dissociated by the end of the dissociation period; and (2) given the sensitive nature of the PDEs, higher concentrations of DMSO or variation in pH were avoided.

Analysis, visualization SPR data

The raw sensorgram data were first imported and analysed in Biacore T200 Evaluation Software (version 2.0, General Electric Company) and Scrubber 2 (version 2.0c, BioLogic Software). The program Inkscape (version 0.48.4) was used for the final typesetting of graphical data.

Acknowledgments

This work is funded by TI Pharma grant T4-302 and the European Commission 7th Framework Programme FP7-HEALTH-2013-INNOVATION-1, PDE4NPD (No. 602666).

References

[1] A.T. Bender, J.A. Beavo, Cyclic nucleotide phosphodiesterases: molecular regulation to clinical use, Pharmacol. Rev. 58 (2006) 488–520.
[2] S.H. Francis, M.A. Blount, J.D. Corbin, Mammalian cyclic nucleotide phosphodiesterases: molecular mechanisms and physiological functions, Physiol. Rev. 91 (2011) 651–690.
[3] S. Uckert, A. Kuthe, C.G. Stief, U. Jonas, Phosphodiesterase isoenzymes as pharmacological targets in the treatment of male erectile dysfunction, World J. Urol. 19 (2001) 14–22.
[4] K.F. Rabe, E.D. Bateman, D. O'Donnell, S. Witte, D. Bredenbroker, et al., Roflumilast–an oral anti-inflammatory treatment for chronic obstructive pulmonary disease: a randomised controlled trial, Lancet 366 (2005) 563–571.
[5] V. Boswell-Smith, D. Spina, C.P. Page, Phosphodiesterase inhibitors, Br. J. Pharmacol. 147 (Suppl 1) (2006) S252–S257.
[6] Y. Shakur, H.P. de Koning, H. Ke, J. Kambayashi, T. Seebeck, Therapeutic potential of phosphodiesterase inhibitors in parasitic diseases, Handb. Exp. Pharmacol. (2011) 487–510.
[7] P.J. Hotez, D.H. Molyneux, A. Fenwick, J. Kumaresan, S.E. Sachs, et al., Control of neglected tropical diseases, N. Engl. J. Med. 357 (2007) 1018–1027.
[8] M. Oberholzer, G. Marti, M. Baresic, S. Kunz, A. Hemphill, et al., The Trypanosoma brucei cAMP phosphodiesterases TbrPDEB1 and TbrPDEB2: flagellar enzymes that are essential for parasite virulence, FASEB J. 21 (2007) 720–731.
[9] S.H. Francis, M.D. Houslay, M. Conti, Phosphodiesterase inhibitors: factors that influence potency, selectivity, and action, Handb. Exp. Pharmacol. (2011) 47–84.
[10] M. Geitmann, G. Dahl, U.H. Danielson, Mechanistic and kinetic characterization of hepatitis C virus NS3 protein interactions with NS4A and protease inhibitors, J. Mol. Recognit. 24 (2011) 60–70.
[11] E. Edink, P. Rucktooa, K. Retra, A. Akdemir, T. Nahar, et al., Fragment growing induces conformational changes in acetylcholine-binding protein: a structural and thermodynamic analysis, J. Am. Chem. Soc. 133 (2011) 5363–5371.
[12] T. Neumann, H.D. Junker, K. Schmidt, R. Sekul, SPR-based fragment screening: advantages and applications, Curr. Top. Med. Chem. 7 (2007) 1630–1642.
[13] W. Huber, A new strategy for improved secondary screening and lead optimization using high-resolution SPR characterization of compound-target interactions, J. Mol. Recognit. 18 (2005) 273–281.
[14] R.L. Thurmond, S.A. Wadsworth, P.H. Schafer, R.A. Zivin, J.J. Siekierka, Kinetics of small molecule inhibitor binding to p38 kinase, Eur. J. Biochem. 268 (2001) 5747–5754.
[15] H. Nordin, M. Jungnelius, R. Karlsson, O.P. Karlsson, Kinetic studies of small molecule interactions with protein kinases using biosensor technology, Anal. Biochem. 340 (2005) 359–368.
[16] I. Navratilova, G. Macdonald, C. Robinson, S. Hughes, J. Mathias, et al., Biosensor-based approach to the identification of protein kinase ligands with dual-site modes of action, J. Biomol. Screen 17 (2012) 183–193.
[17] K.M. Orrling, C. Jansen, X.L. Vu, V. Balmer, P. Bregy, et al., Catechol pyrazolinones as trypanocidals: fragment-based design, synthesis, and pharmacological evaluation of nanomolar inhibitors of trypanosomal phosphodiesterase b1, J. Med. Chem. 55 (2012) 8745–8756.
[18] A.R. Blaazer, K.M. Orrling, A. Shanmugham, C. Jansen, L. Maes, et al., Fragment-based screening in tandem with phenotypic screening provides novel antiparasitic hits, J. Biomol. Screen 20 (2015) 131–140.
[19] J.E. Schultz, Structural and biochemical aspects of tandem GAF domains, Handb. Exp. Pharmacol. (2009) 93–109.
[20] J. Pandit, M.D. Forman, K.F. Fennell, K.S. Dillman, F.S. Menniti, Mechanism for the allosteric regulation of phosphodiesterase 2A deduced from the X-ray structure of a near full-length construct, Proc. Natl. Acad. Sci. U. S. A. 106 (2009) 18225–18230.
[21] C.C. Heikaus, J. Pandit, R.E. Klevit, Cyclic nucleotide binding GAF domains from phosphodiesterases: structural and mechanistic insights, Structure 17 (2009) 1551–1557.
[22] D.H. Maurice, H.M. Ke, F. Ahmad, Y.S. Wang, J. Chung, et al., Advances in targeting cyclic nucleotide phosphodiesterases, Nat. Rev. Drug Discov. 13 (2014) 290–314.
[23] Q. Huai, H. Wang, Y. Sun, H.Y. Kim, Y. Liu, et al., Three-dimensional structures of PDE4D in complex with roliprams and implication on inhibitor selectivity, Structure 11 (2003) 865–873.
[24] C. Jansen, H. Wang, A.J. Kooistra, C. de Graaf, K. Orrling, et al., Discovery of novel Trypanosoma brucei phosphodiesterase B1 inhibitors by virtual screening against the unliganded TbrPDEB1 crystal structure, J. Med. Chem. 56 (5) (2013) 2087–2096.
[25] R. Zoraghi, T. Seebeck, The cAMP-specific phosphodiesterase TbPDE2C is an essential enzyme in bloodstream form Trypanosoma brucei, Proc. Natl. Acad. Sci. U. S. A. 99 (2002) 4343–4348.
[26] A. Shanmugham, A. Bakayan, P. Voller, J. Grosveld, H. Lill, et al., The hydrophobic core of twin-arginine signal sequences orchestrates specific binding to Tat-pathway related chaperones, PLoS One 7 (2012) e34159.
[27] L. Joss, T.A. Morton, M.L. Doyle, D.G. Myszka, Interpreting kinetic rate constants from optical biosensor data recorded on a decaying surface, Anal. Biochem. 261 (1998) 203–210.
[28] M.A. Wear, A. Patterson, K. Malone, C. Dunsmore, N.J. Turner, et al., A surface plasmon resonance-based assay for small molecule inhibitors of human cyclophilin A, Anal. Biochem. 345 (2005) 214–226.

[29] D.A. Edwards, Steric hindrance effects on surface reactions: applications to BIAcore, J. Math. Biol. 55 (2007) 517–539.
[30] P. Wang, J.G. Myers, P. Wu, B. Cheewatrakoolpong, R.W. Egan, et al., Expression, purification, and characterization of human cAMP-specific phosphodiesterase (PDE4) subtypes A, B, C, and D, Biochem. Biophys. Res. Commun. 234 (1997) 320–324.
[31] M. Salanova, S.C. Jin, M. Conti, Heterologous expression and purification of recombinant rolipram-sensitive cyclic AMP-specific phosphodiesterases, Methods 14 (1998) 55–64.
[32] R. Diaz-Benjumea, S. Laxman, T.R. Hinds, J.A. Beavo, A. Rascon, Characterization of a novel cAMP-binding, cAMP-specific cyclic nucleotide phosphodiesterase (TcrPDEB1) from Trypanosoma cruzi, Biochem. J. 399 (2006) 305–314.
[33] M. Conti, Phosphodiesterases and cyclic nucleotide signaling in endocrine cells, Mol. Endocrinol. 14 (2000) 1317–1327.
[34] M. Conti, W. Richter, C. Mehats, G. Livera, J.Y. Park, et al., Cyclic AMP-specific PDE4 phosphodiesterases as critical components of cyclic AMP signaling, J. Biol. Chem. 278 (2003) 5493–5496.